

The clustering of galaxies in the SDSS-III Baryon Oscillation Spectroscopic Survey: mock galaxy catalogues for the low-redshift sample

Marc Manera,^{1,2★} Lado Samushia,^{2,3,4} Rita Tojeiro,² Cullan Howlett,²
Ashley J. Ross,² Will J. Percival,² Hector Gil-Marín,² Joel R. Brownstein,⁵
Angela Burden² and Francesco Montesano⁶

¹University College London, Gower Street, London WC1E 6BT, UK

²Institute of Cosmology and Gravitation, Portsmouth University, Dennis Sciama Building, Portsmouth PO1 3FX, UK

³National Abastumani Astrophysical Observatory, Ilia State University, 2A Kazbegi Ave., GE-1060 Tbilisi, Georgia

⁴Department of Physics, Kansas State University, 116 Cardwell Hall, Manhattan, KS 66506, USA

⁵Department of Physics and Astronomy, University of Utah, 115 S 1400 E, Salt Lake City, UT 84112, USA

⁶Max-Planck-Institut für Extraterrestrische Physik, Giessenbachstraße, D-85748 Garching, Germany

Accepted 2014 November 17. Received 2014 November 17; in original form 2014 January 16

ABSTRACT

We present 1000 mock galaxy catalogues (mocks) for the analysis of the low-redshift sample (LOWZ; effective redshift $z \sim 0.32$) of the Baryon Oscillation Spectroscopic Survey (BOSS) Data Releases 10 and 11. These mocks have been created following the PTHalos method revised to include new developments. The main improvement is the introduction of a redshift dependence in the halo occupation distribution in order to account for the change of the galaxy number density with redshift. These mock galaxy catalogues are used in the analyses of the LOWZ galaxy clustering by the BOSS collaboration.

Key words: galaxies: haloes – galaxies: statistics – large-scale structure of Universe.

1 INTRODUCTION

The Baryon Oscillation Spectroscopic Survey (BOSS; Dawson et al. 2013) is a spectroscopic survey that uses imaging data from Sloan Digital Sky Survey III (SDSS-III; Eisenstein et al. 2011) to map over 1.35 million galaxies covering an unprecedented volume of the Universe over an area of approximately a quarter of the sky. The BOSS Data Release 11 (DR11; Anderson et al. 2014) contains 1277 503 galaxies covering 8498 deg², which, assuming a concordance Λ cold dark matter (Λ CDM) model, results in an effective volume of 8.4 Gpc³, the largest ever surveyed at this density.

BOSS targets two distinct galaxy samples: the CMASS sample, a high-redshift sample $0.4 \lesssim z \lesssim 0.7$ that selects galaxies with roughly a constant stellar mass, and a low-redshift sample (LOWZ) $0.2 \lesssim z \lesssim 0.45$ that targets galaxies following an algorithm close to that designed for luminous red galaxies (LRGs) in SDSS-I/II (Eisenstein et al. 2001). Each of the DR11 samples has been used to fit the position of the baryon acoustic oscillation (BAO) feature, constraining the cosmic distance scale at 2 per cent for LOWZ (Tojeiro et al. 2014) and 1 per cent in CMASS (Anderson et al. 2014). The latter is the most precise distance constraint ever obtained from a galaxy survey.

The generation of mock galaxy catalogues (mocks) is an essential component to the analysis of the data from any galaxy surveys. Mocks are required for an accurate understanding of the sampling errors and the systematic errors of the clustering measurements, including the effects of cosmic variance, non-linear evolution, scale-dependent bias, redshift distortions, and discreteness effects. They also enable detailed testing of analysis pipelines. For a particular survey, mock galaxy catalogues mimic the survey geometry, the number density of objects and their selection. All key science analyses of large-scale galaxy clustering from BOSS Data Release 9 (DR9) relied heavily on the mock galaxy catalogues presented in Manera et al. (2013). Science analyses of ongoing and future surveys such as the Dark Energy Survey (DES),¹ or in the near future Hobby–Eberly Telescope Dark Energy Experiment (HETDEX; Hill et al. 2004), Dark Energy Spectroscopic Instrument (DESI; Levi et al. 2013), *Euclid* (Laurejis et al. 2011), and Large Synoptic Survey Telescope (LSST; LSST Science Collaboration 2009) will also require a large suite of mock galaxy catalogues.

Ideally a set of high-resolution N -body cosmological simulations, including hydrodynamics, would be run to generate the mock galaxy catalogues, but in practise the computational time that this would require is exceedingly expensive. Semi-analytical

★E-mail: m.miret@ucl.ac.uk

¹<http://www.darkenergysurvey.org>

models of galaxy formation in combination with dark matter N -body simulations would have the same problem, as a computationally expensive N -body simulation would need to be run for each realization. For this reason other methods to generate a large number of mock galaxy catalogues quickly have been developed.

Manera et al. (2013), inspired by Scoccimarro & Sheth (2002), developed the PThalos method to generate fast mock galaxy catalogues. The three main steps are the following. (i) Generate a dark matter field using second-order Lagrangian perturbation theory (2LPT). The input required for this is an initial power spectrum (that can be generated with CAMB) and the target redshift. (ii) Find haloes in the dark matter field, using a group finder [in our case friends-of-friends (FoF)] with a prescription that is calibrated against numerical simulations. (iii) Populate the haloes with galaxies using a halo occupation distribution (HOD) fitted to the observed clustering of galaxies (see Section 3 for details). This method was used to create mock catalogues for the BOSS CMASS DR9 sample, which were used in analyses by Anderson et al. (2012, 2014), Tojeiro et al. (2012), Samushia et al. (2013), Reid et al. (2012), and Sánchez et al. (2014).

Other methods have also been developed to generate fast galaxy mocks. Monaco et al. (2013) and Monaco, Theuns & Taffoni (2002) use the collapse times of dark matter particles in the Lagrangian field smoothed at several scales to fragment the dark matter field into haloes, giving clustering results similar to that of PThalos. It has also been suggested that N -body simulations could be run with low time resolution. These runs are 2–3 times slower than the methods based on a single field, but still at least within an order of magnitude or two faster than full N -body simulations. Tassev, Zaldarriaga & Eisenstein (2013) suggested using 2LPT analytically at large scales, and White, Tinker & McBride (2014) advocate to run a particle-mesh simulation in small number of steps. They obtain an improved accuracy on the mass function and clustering with respect to the perturbation-theory-based methods.

Finally, in order to increase the mass range of the haloes from which galaxies are drawn in mocks, one can use the conditional halo bias as a function of the local halo density (de la Torre & Peacock 2013), or use the halo mass function of higher resolution N -body simulations and implement that as a function of the local matter density in a lower resolution run (Angulo et al. 2014), or also, alternatively, combine the 2LPT approach for large scales with the spherical collapse model for small scales (Kitaura & Heß 2013). We do not apply such methods here and use a mapping between the mocks and corresponding N -body simulations instead (see Section 3 for details).

Notice that our methodology does not include baryonic feedback as is the case of most cosmological simulations and all of the methods that generate fast mock galaxy catalogues. Baryonic feedback processes are necessarily small-scale in nature. However they can affect large-scale clustering for objects selected based on properties that are affected by such processes. For example, active galactic nuclei (AGN) winds blowing baryonic material away from haloes will increase the bias of haloes selected at a fixed stellar mass: these will correspond to higher dark matter mass. Changes in the clustering at large scales, estimated from semi-analytic models, are expected to be lower than 5 per cent (Angulo et al. 2014), although for our redshift and galaxy density it would be much lower in our case. Typically these differences are reabsorbed by the HOD, making the error of missing baryon physical subdominant in our analysis. Apart from such a change in apparent large-scale bias, baryon processes are expected to only change the shape of the power spectrum on small scales $k \gtrsim 0.3$ (e.g. Van Daalen et al. 2011). These scales

are not those that we are interested in, or at which the mocks are designed to be accurate.

In this paper we present 1000 mock galaxy catalogues for the LOWZ DR10 and DR11 BOSS galaxy samples. These mocks were produced using the PThalos method developed in Manera et al. (2013) but with a redshift dependence in the HOD of galaxies in haloes in order to account for the change of the galaxy number density in redshift. The mocks are fitted to the LOWZ sample clustering presented in Tojeiro et al. (2014) and the masks applied to the mocks mimic the survey geometry, observational completeness, and small-scale features such as patches of bad imaging and bright stars. These mocks have been used to provide covariance matrices and enable the study the systematic and statistical uncertainty on the BAO scale measurements presented in Anderson et al. (2014), Sánchez et al. (2014), and Chuang et al. (2013). The mocks will be made publicly available.²

This paper is organized as follows. In Section 2 we introduce the LOWZ sample. We summarize the PThalos method and discuss the geometry of the sample and the masks in Section 3. The HOD fitting is presented in Section 4. In Section 5 we explain the results and conclude in Section 6. Finally, table with the covariance matrices of the LOWZ sample correlation function is provided.

2 BOSS LOWZ GALAXY SAMPLE

BOSS uses SDSS CCD photometry (Gunn et al. 1998, 2006) from five passbands (u, g, r, i, z ; e.g. Fukugita et al. 1996) to select targets for spectroscopic observation. The LOWZ galaxy sample of BOSS targets galaxies with an algorithm that follows closely the one designed in SDSS-I/II for LRGs, described in Eisenstein et al. (2001), but extending to fainter magnitudes to increase the number density. This data set has already been used by Anderson et al. (2014), Parejko et al. (2013), and Tojeiro et al. (2014).

The LOWZ Data Release 10 (DR10) covers a total area of 5635 deg² and is split into two separate contiguous regions. One is in the northern Galactic cap (NGC) and covers 4205 deg². The other is in the southern Galactic cap (SGC) and covers 1430 deg². The total LOWZ DR10 sample has 218 905 galaxies with $0.15 \lesssim z \lesssim 0.43$. DR11 covers, respectively, a total area of 7998 deg² (5793 deg² in the NGC and 2205 deg² in the SGC) and has a total of 313 780 galaxies. The NGC footprint is smaller than that of the CMASS sample as the final target algorithm was not used for LOWZ during the first 9 months of BOSS observations. The footprint of the LOWZ sample is shown in Fig. 1.

Parejko et al. (2013) studied the small-scale clustering of the LOWZ sample and showed that the LOWZ galaxies occupy haloes of typical mass of $\sim 5 \times 10^{13} h^{-1} M_{\odot}$, and galaxy bias $b \sim 2.0$. The large-scale clustering of the LOWZ sample is presented in Tojeiro et al. (2014), where the observational systematics of the sample are studied in detail. The effective isotropic distance at $z = 0.32$, $D_V = [cz(1+z)^2 D_A^2 / H]^{\frac{1}{3}}$, where H is the Hubble parameter and D_A the angular diameter distance, has been measured using the LOWZ BAO peak with an accuracy better than 2 per cent. The cosmological implications of this measurement when combined with the BAO measurement from the CMASS sample are presented in Anderson et al. (2014). Both papers have used the PThalos mocks galaxy catalogues for the covariance matrices and analysis of errors.

² www.marcmanera.net/mocks/

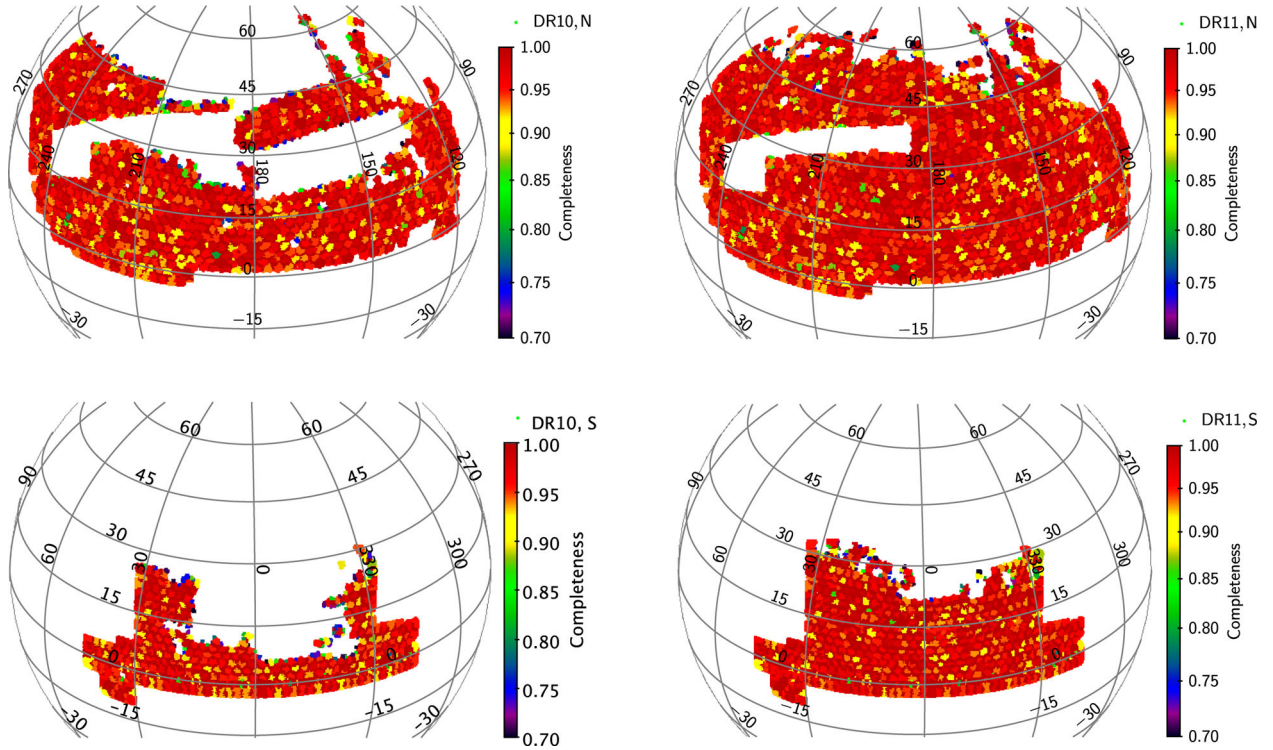


Figure 1. DR10 (left) and DR11 (right) survey footprints in equatorial coordinates. Northern Galactic caps on the top and southern Galactic caps on the bottom. The colour code shows the completeness of each sector.

3 METHOD

We have created 1000 mock galaxy catalogues for the LOWZ DR10 and DR11 galaxy samples. We use a method similar to that of Manera et al. (2013), adapted to a lower redshift and with several improvements. The mocks are such that covariance matrices can be computed and the methods of analysis of the galaxy clustering can be tested for bias and relative accuracy. The steps that we took in generating these PTHalos mocks can be summarized as follows.

3.1 Dark matter

We have run 500 dark matter particle fields based on 2LPT, using the publicly available code `2LPTIC`.³ The matter fields were generated at redshift $z = 0.32$, which is the effective pair-weighted redshift of the LOWZ sample. The matter realizations have been generated in a cubical box of size $L = 2400 h^{-1}$ Mpc with $N = 1280^3$ particles, for a Λ CDM cosmology with parameters $\Omega_m = 0.274$, $\Omega_\Lambda = 0.726$, $\Omega_b = 0.04$, $h = 0.7$, $\sigma_8 = 0.8$, and $n_s = 0.95$, giving a particle mass $M_p = 50.1 \times 10^{10} M_\odot h^{-1}$. The input power spectrum has been smoothed with a cut-off as in Manera et al. (2013) as it helps the clustering of small haloes. These cosmological parameters are the same as the standard fiducial choices used in BOSS analyses (e.g. White et al. 2011; Anderson et al. 2012, 2014).

3.2 Haloes

Haloes have been identified in the dark matter field using a FoF halo finder algorithm (Davis et al. 1985) which percolates in a halo all the particles that can be linked by within a given linking length l .

The value of the linking length used in N -body simulations varies in the literature, the most common value being $l = 0.2$ times the mean interparticle distance. For a 2LPT dark matter field the value of the linking length has to be appropriately changed in accord with the 2LPT dynamics. In the spherical collapse approximation both values can be related as follows (Manera et al. 2013):

$$l_{2\text{LPT}} = l_{N\text{-body}} \left(\frac{\Delta_{\text{vir}}^{N\text{-body}}}{\Delta_{\text{vir}}^{2\text{LPT}}} \right)^{1/3}, \quad (1)$$

where $\Delta_{\text{vir}}^{N\text{-body}}$ and $\Delta_{\text{vir}}^{2\text{LPT}}$ are the N -body and 2LPT virial overdensities. For the N -body haloes we take the value of Bryan & Norman (1998) fit:

$$\Delta_{\text{vir}}^{\text{sim}} = [18\pi^2 + 82(\Omega_m(z) - 1) - 39(\Omega_m(z) - 1)^2] / \Omega_m(z), \quad (2)$$

where $\Omega_m(z) = \Omega_m(1+z)^3 H(0)/H(z)$, and $H(z)$ is the Hubble expansion value at redshift z . $\Delta_{\text{vir}}^{N\text{-body}} = 264$ in our fiducial cosmology. For the 2LPT haloes we take $\Delta_{\text{vir}}^{2\text{LPT}} = 35.4$. This value comes from the relation between the linear and non-linear density in 2LPT:

$$\Delta_{\text{vir}}^{2\text{LPT}} = \delta_{\text{NL}}^{2\text{LPT}} + 1 \simeq (1 - \delta_0 D_1 / 3 - \delta_0^2 D_1^2 / 21)^{-3}, \quad (3)$$

where $\delta_0 D_1 = 1.68$ is the value of the linear density fluctuation at collapse, and δ_{NL} , its non-linear value.

Applying the above equations, we use the linking length value $l = 0.39$ for haloes at redshift $z = 0.32$. As the value is approximate, and 2LPT lacks small-scale power, the halo mass function recovered would not completely match that of an N -body simulation. Therefore, following Manera et al. (2013), we reassigned the masses of the haloes, while keeping their positions and rank-order in mass, such that we recover the Tinker et al. (2008) mass function for this cosmology. This method has been shown to match the clustering of haloes in N -body simulations within 10 per cent accuracy.

³ <http://www.marcmanera.net/2LPT/>

In our sample, for a random chosen galaxy, the typical correction of its host halo is about 30 per cent of the mass, and the largest corrections are of order 50 per cent.

3.3 Galaxies

We assign galaxies to haloes by means of an HOD (Peacock & Smith 2000; Scoccimarro et al. 2001; Berlind & Weinberg 2002) functional form with five parameters, as used by Zheng et al. (2007). The mean number of galaxies in a halo of mass M is the sum of the mean number of central galaxies plus the mean number of satellite galaxies, $\langle N(M) \rangle = \langle N_{\text{cen}}(M) \rangle + \langle N_{\text{sat}}(M) \rangle$, where

$$\langle N_{\text{cen}} \rangle = \frac{1}{2} \left[1 + \text{erf} \left(\frac{\log M - \log M_{\text{cut}}}{\sigma_{\log M}} \right) \right],$$

$$\langle N_{\text{sat}} \rangle = \langle N_{\text{cen}} \rangle \left(\frac{M - M_0}{M_1} \right)^\alpha, \quad (4)$$

and $\langle N_{\text{sat}} \rangle = 0$ if the halo mass has $M < M_0$. In this parametrization M_{cut} and M_1 are the typical halo masses for having, respectively, order of one central and one satellite galaxy.⁴ The HOD parameters are calibrated to fit the observational data (see Section 4). Galaxies in haloes are given the velocity of the halo, i.e. the velocity of the centre of mass of the particles in the halo, plus a dispersion velocity from a Gaussian distribution with an amplitude given by the mass of the halo and the virial theorem. Galaxies that are below our lower halo mass limit of $5 \times 10^{12} M_\odot h^{-1}$ (7 per cent of the total) are assigned randomly to dark matter particles that do *not* belong to haloes. This is different from the CMASS mocks in Manera et al. (2013) where we randomly assigned these galaxies to any dark matter particle. More importantly, we have allowed the HOD to depend on the number density of galaxies, and fitted the HOD *simultaneously* with the number density as a function of redshift, therefore, we have *not* subsampled the galaxy field a posteriori to match the LOWZ distribution. The details of the fitting procedure are explained in Section 4.

3.4 Mask: geometry

BOSS covers regions of the sky in the two Galactic hemispheres. Fig. 1 shows the NGC and the SGC observed footprints for the LOWZ Data Release 10 and 11 (DR10, DR11), the latter more than double the areas observed by BOSS in DR9.

As with the data, the footprints of the mock galaxy catalogues exclude vetoed regions, which amounts to about 5 per cent of the total area covered. These regions are generally small and have been removed for a variety of reasons including regions with bad photometry, failure of the point spread function (PSF) modelling, timing out errors in the pipeline reduction, or regions around bright stars, or around objects that have been highly prioritized, since a galaxy cannot be observed within the fibre collision radius of these points. For more detailed information of the veto mask see Anderson et al. (2012) and SDSS DR10 documentation.

In Table 1 we show the areas of the NGC and SGC of the LOWZ DR10 and DR11 mock galaxy catalogues. There are small differences (less than 0.5 per cent) between the areas of the mocks and of the data, which result because of ‘last minute’ changes to the data mask used. The effect of these differences is insignificant. The effective area is the area used weighted by the target completeness.

⁴ In this paper log always stands for base-10 logarithm.

Table 1. Areas of the LOWZ sample mock galaxy catalogues for the NGC and SGC.

LOWZ DR10	NGC	SGC
Total area/deg ²	4222	1429
Veto area/deg ²	251	58
Used area/deg ²	3971	1371
Effective area/deg ²	3840	1331
LOWZ DR11	NGC	SGC
Total area/deg ²	5787	2204
Veto area/deg ²	335	89
Used area/deg ²	5452	2115
Effective area/deg ²	5287	2060

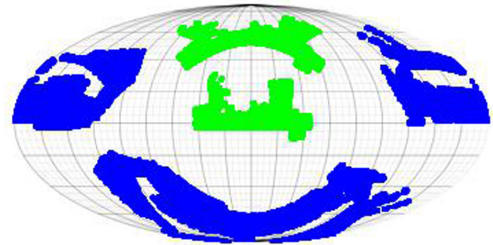


Figure 2. Footprints of the LOWZ DR10 NGC (blue, bigger areas) and SGC (green, smaller areas) mock galaxy catalogues. Two of each can fit without overlap in the celestial sphere. The same is true for the DR11 footprints.

Regarding the geometry of the LOWZ sample, it is worth noticing that it is possible to fit two samples of the NGC and SGC footprints in the celestial sphere without overlap. We have taken advantage of that when creating our mock galaxy catalogues. In this way we only needed 500 matters field to generate 1000 mocks. In order to get two footprints within the same matter run, we convert the right ascension, RA, and declination, Dec., to Cartesian coordinates and then rotate about the y-axis. Fig. 2 shows two NGC and two SGC footprints. The second footprints of the NGC and SGC are obtained by rotating the previous ones, respectively, with $\alpha = -120^\circ$ and -55° . Since there is no overlap between the footprints and the number of pairs at the scales of interest between different footprints is negligible, thus each mock can be taken as an independent realization.

3.5 Mask: completeness

The mocks have been created taking into account the completeness of the sample observed at every sector in the sky, as measured from the data. We do not reposition plates for each mock as if we were performing actual observations. The mock galaxies have been subsampled to mimic variations in the target completeness, redshift failures, and close pair completeness. Close pair completeness refers to the case where a spectroscopic redshift of a galaxy is not available due to the fact that is within 62 arcsec of another galaxy, meaning that two fibres cannot be placed on both galaxies simultaneously. The effective areas of the mocks, that result from weighting by a measure of target completeness, C_{BOSS} , as defined in Anderson et al. (2012) are shown in Table 1. For detailed numbers of galaxies, missed targets, and areas of the LOWZ galaxy sample see Tojeiro et al. (2014).

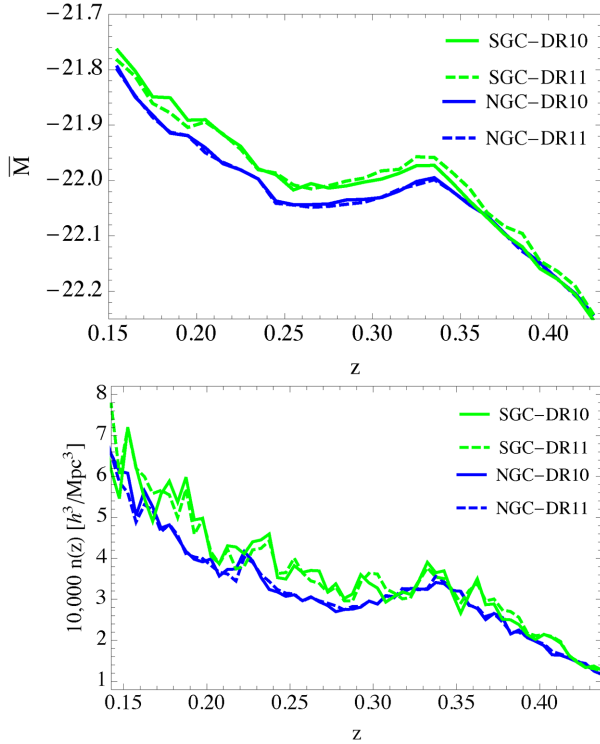


Figure 3. Top: average of the absolute magnitude of the LOWZ DR10 (solid line) and DR11 (dashed line) galaxy samples. Bottom: number density of galaxies of the LOWZ DR10 (solid line) and DR11 (dashed line) galaxy samples. In both panels the lower (blue) lines show the NGC sample and the higher (green) lines the SGC.

4 MODELLING THE GALAXY DISTRIBUTION

4.1 HOD(z)

Given a HOD set of parameters the number density of galaxies is fixed; it can be obtained as an integration of the halo mass function (which depends on the redshift) weighted by the HOD. Previous mock galaxy catalogues based on populating haloes from a cosmological time slice by means of an HOD have, by construction, a constant number density of galaxies. Consequently, to mimic the number density as a function of redshift, the number of galaxies must be subsampled a posteriori (Manera et al. 2013; Xu et al. 2013; McBride, in preparation).⁵ Randomly subsampling a distribution of galaxies would not change any of its fundamental properties apart from the number density itself.

In the top panel of Fig. 3 we show the average absolute magnitude of the (k -corrected r band) galaxies in the LOWZ sample for DR10 and DR11. We see that the average magnitude of the sample varies with redshift for both the NGC and SGC. Moreover the shape as a function of redshift is similar to that of the number density, which we show in the bottom panel of Fig. 3. This suggests that the HOD parameters are *not* likely to be well approximated as constant with redshift.

Notice that the SGC and the NGC are disconnected regions. The offset between the photometric calibration between the two regions is the main cause of the differences between their number densities

(Ross et al. 2012; Reid et al., in preparation), consequently we fit both regions separately.

In this paper we want to improve on the mocks by allowing the HOD parameters to vary as a function of redshift. Fitting a different HOD parameters in redshift slices would not constrain the HOD parameters sufficiently, so we have chosen instead to include the redshift dependence through a fixed dependency of the HOD parameters on the number density of galaxies. This dependency is based on previous studies, as we now describe.

Parejko et al. (2013) report a compilation of the M_{cut} and M_1 HOD parameters from various papers in the literature based on a variety of different galaxy samples. While the functional form of the HOD used in these papers varies, they are sufficiently similar to allow for a comparison between the derived parameters and thus study the evolution of the HOD. We have used the data from table A1 in Parejko et al. (2013) to fit a log-linear dependence of M_{cut} and M_1 as a function of the number density of galaxies used in each paper. In Fig. 4, we show the data and our best fits:

$$\log M_{\text{cut}} = \log M_{\text{cut}}^0 + S_{\text{cut}} \bar{n},$$

$$\log M_1 = \log M_1^0 + S_1 \bar{n}, \quad (5)$$

where $\log M_{\text{cut}}^0 = 9.90 \pm 0.12$, $S_{\text{cut}} = -0.925 \pm 0.035$, $\log M_1^0 = 10.81 \pm 0.12$, and $S_1 = 0.928 \pm 0.037$.

We have considered data from the publications that include the parameters α , $\kappa = M_0/M_1$, or $\sigma_{\log M}$, and found no significant dependency of these parameters on the number density of galaxies. Consequently, for simplicity, when fitting the HOD parameters for our mocks, we keep these parameters constant as a function of redshift. Future mocks could improve on this by allowing these parameters to vary. For M_{cut} and M_1 we have fixed the tilts S_{cut} and S_1 to the best-fitting values given the previous data and fitted only the amplitudes M_{cut}^0 and M_1^0 to the BOSS data. For a redshift and luminosity dependence of the HOD see also Zheng, Coil & Zehavi (2007), Coupon et al. (2012), Tinker et al. (2013), and Hong et al. (2014).

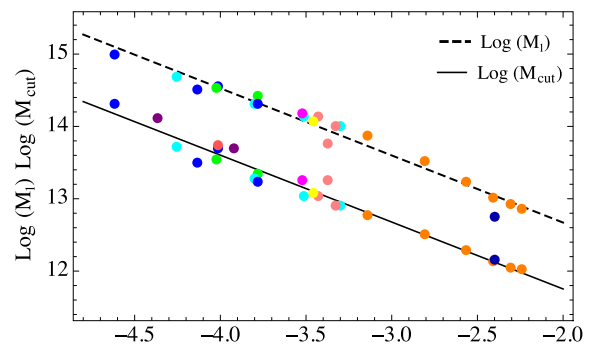


Figure 4. HOD parameters M_{cut} and M_1 as a function of the number density of galaxies. The points are from the list of table A1 in Parejko et al. (2013). Blue: SDSS LRG (2PCF), Zheng et al. (2009) and Mandelbaum et al. (2006); cyan: SDSS LRG (photo- z , BCL), Blake, Collister & Lahav (2008); pink: SDSS LRG (photo- z , PW), Padmanabhan et al. (2009); dark blue: Combo-17, Phleps et al. (2006); purple: SDSS LRG (lensing), Mandelbaum et al. (2006); red: SDSS LRG (3PCF), Kulkarni et al. (2007); orange: NDWFS, Brown et al. (2008); green: 2SLAQ, Wate et al. (2008) and Kulkarni et al. (2007); yellow: BOSS CMASS, White et al. (2011); magenta: LOWZ, Parejko et al. (2013).

⁵ <http://lss.phy.vanderbilt.edu/lasdams/download.html>

4.2 Fit to $n(z)$

The actual number density of observed LOWZ galaxies varies as a function of redshift for two main reasons. The principal effect is due to the colour and magnitude cuts of the target selection that induce a smooth redshift dependence. In addition, there are ‘high-frequency’ variations in redshift that come from observing a particular volume of the Universe, i.e. cosmic variance. The shot-noise contribution from being a sample with a finite number of galaxies is subdominant with respect to the cosmic variance.

We creating our suite of mock catalogues, we aim to an average redshift distribution that matches the smooth component of the observed redshift profile without the noisy component that is specific to the observed sample. The noisy contribution is accounted for as each mock is a different realization of our Universe, within our fiducial cosmology.

We have therefore smoothed the observational galaxy redshift distribution to obtain the target $n(z)$ to which we fit the HOD of the mock galaxy catalogues. The smoothed $n(z)$ is a cubic spline curve with seven nodes. The number of nodes and their $n(z)$ values have been determined with a minimization process. First, we have estimated a covariance matrix of $n(z)$, in bins of 0.05, from a preliminary version of the mocks that already included a redshift-dependent number density. Then, using this covariance matrix, we have fitted a set of cubic splines to the observed $n(z)$, each spline with a different number of nodes. For each of these splines we have set the $n(z)$ values by minimizing the χ^2 against the observed $n(z)$. As expected the goodness of fit increases with the number of nodes but at the expense of mimicking all the little wiggles that are induced by cosmic variance. Consequently, we have used the lower number of nodes that fit the data with $\chi^2 \sim 1$ per degree of freedom.

We have found that, for the NGC, seven nodes in the range $0.1175 < z < 0.4425$ fit well the redshift distribution, so we have used this number for our $n(z)$ spline. The redshift range is broader than the one we use for our LOWZ sample $0.15 < z < 0.43$ to allow for redshift-space distortions that may cross the redshift boundary. We have fitted the SGC with the same number of nodes, as we expect the smooth component of $n(z)$ to be similar in the two hemispheres and the NGC measured $n(z)$ has a higher signal-to-noise ratio (see Tojeiro et al. 2014 for a discussion of NGC and SGC differences).

4.3 HOD fit

We have set the HOD parameters by minimizing the χ^2 value of the power spectrum and the number density. The joint χ^2 is thus the addition of the two respective contributions:

$$\chi^2 = \sum_{i,j} (P^m(k_i) - P^d(k_i)) C_{i,j}(P)^{-1} (P(k_j)^m - P(k_j)^d) + \sum_{st} (n^m(z_s) - n^d(z_s)) C_{s,t}(n)^{-1} (n(z_t)^m - n(z_t)^d), \quad (6)$$

where $P(k_l)$ is the value of the power spectrum at wavenumber bin l , and $C_{i,j}(P)$ is the covariance matrix of the power spectrum. In the same manner $n(z_l)$ is the value of the number density at redshift bin l , and $C_{s,t}(n)$ the covariance of the number density of galaxies. The labels d and m stand for data and mocks. We have fitted $P(k)$ in the range $0.02 < k < 0.15$ and $n(z)$ in the range $0.15 < z < 0.43$. For each HOD set of parameters that we have run we took the mock power spectrum and number density to be the mean of 10 realizations for the NGC and 20 for the SGC. In this way we reduce the effect of fitting the data with only one mock catalogue. We have

Table 2. HOD values for the LOWZ mock galaxy catalogues for the NGC and SGC.

Param	NGC	SGC
$\log M_{\text{cut}}$	13.20	13.14
$\log M_1$	14.32	14.58
$\log M_0$	13.24	13.43
$\sigma_{\log M}$	0.62	0.55
α	0.93	0.93
χ^2	49	30

used 20 mocks for the SGC and then for the NGC in order to have a similar number of galaxies in both cases.

To minimize the χ^2 we have used the simplex algorithm of Nelder & Mead (1965). This method constructs a multidimensional simplex with vertices given by the initial guess of the HOD parameters and a certain step size. By a series changes of the position of the vertex with worst χ^2 the simplex moves in the parameter space until it brackets the minimum within a given volume.

For the covariance matrices we have used an estimation of a preliminary version of the mocks that had been created in the same manner starting with the HOD parameters of Parejko et al. (2013). With this covariance matrix we then minimized the HOD, separately for the NGC and SGC, obtaining the best fits in Table 2, where $\log M_{\text{cut}}$, $\log M_1$, and $\log M_0$ are the values of the HOD parameters when in equation (5) we set $n(z) = 2.98 \times 10^{-4} h^3 \text{Mpc}^{-3}$ and S_{cut} and S_1 are, respectively, -0.925 and -0.928 . As the HOD that we are using has five free parameters there is some room for the best fit to vary depending on the initial guess at which the fitting starts as well as the particular set mock realizations used to fit the data. We also expect the observational HOD to be different due to the fact that 7 per cent of our galaxies are not in resolved haloes in our simulation. The values we have found for the HOD parameters are within 1σ of the mean of the full sample in Parejko et al. (2013). The recovered χ^2 values for our best-fitting HOD models show they are a good fit to the data. Indeed, since we have 88 bins in total (32 from $P(k)$ and 56 from $n(z)$), the χ^2 values are less than the number of degrees of freedom, and thus a good fit for the purposes of creating mocks for covariance matrices and clustering data analysis.

In Fig. 5 we show the number density of galaxies in the DR10 LOWZ sample for the NGC and the SGC, with errors displaying

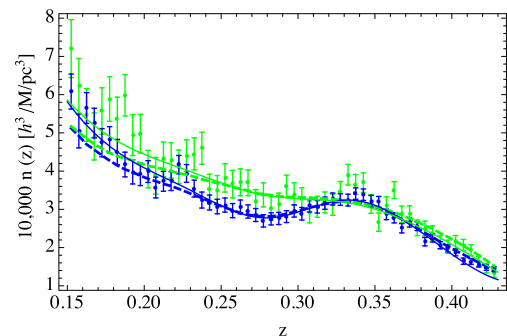


Figure 5. Number density of galaxies of the LOWZ DR10 galaxy sample for the NGC (blue dots, lower values) and the SGC (green dots, higher values). Error bars show the rms of the 1000 mock galaxy catalogues. The solid lines are fits to the data. The mock galaxy catalogues $n(z)$ are shown in dashed lines; all the redshift dependence of the mocks $n(z)$ comes through the variation of the HOD.

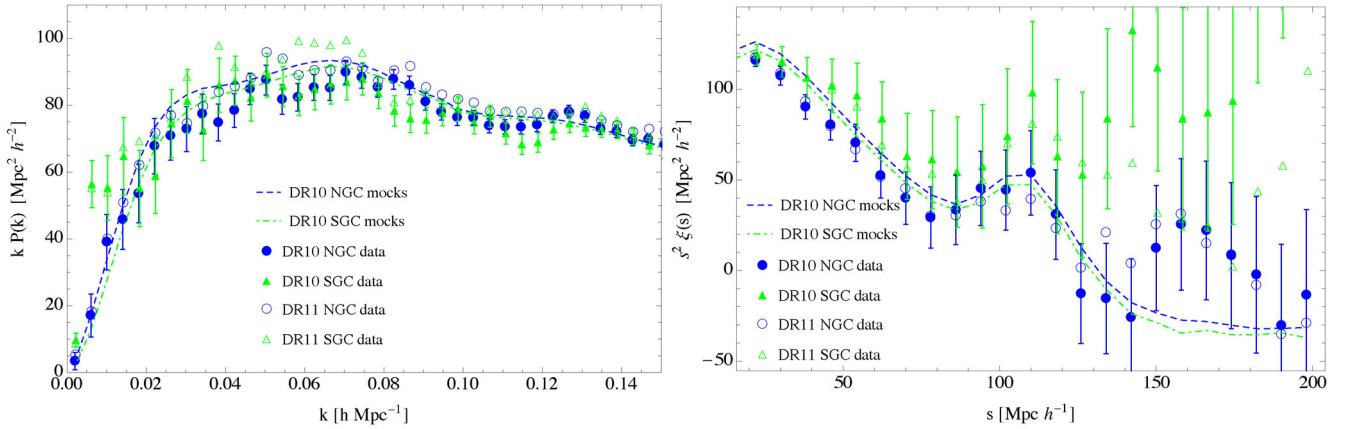


Figure 6. Power spectrum and correlation function of the LOWZ galaxy sample. The DR10 NGC and SGC measurements are shown as blue solid circles and green solid triangles, respectively, with sample errors from the dispersion of the mock galaxy catalogues. DR11 clustering is displayed in open symbols. The mean values of the mocks are shown for the NGC and SGC as dashed (blue) and dot-dashed (green) lines.

the rms of the 1000 mock galaxy catalogues. The solid lines show the mean of the targeted $n(z)$ that comes from the seven-node spline fit to the data, and the dashed lines shows the mean $n(z)$ of the mock galaxy catalogues. The number density of the mocks has not been subsampled and its redshift dependence comes only through equation (5) after fitting for the HOD parameters. We recover the redshift distribution for $z > 0.2$ quite well. At lower redshift the differences come from the fact that the log-linear (or constant) dependence of the HOD mass parameters as a function of $n(z)$ is an approximation to the true HOD as function of redshift.

Following the methods outlined in Sections 3 and 4 we have created 1000 mock galaxy catalogues for the LOWZ DR10 and DR11 galaxy sample. Since both releases have the same targeting their clustering and redshift distributions are very similar. We have consequently used the same halo fields and HOD parameters for both releases, those fitted with DR10 data.

5 RESULTS

In the left-hand panel of Fig. 6 we show the power spectrum of the DR10 LOWZ galaxy sample with errors from the mocks, both for the NGC (blue solid circles) and the SGC (green solid circles). The DR11 values are set as open symbols. We have used the (Feldman, Kaiser & Peacock 1994, hereafter FKP) estimator. The mean of the mock catalogues is shown by the solid lines. There is a good fit between the data and the mock catalogues for $k > 0.02 h\text{Mpc}^{-1}$, which is the region in which we have fitted the HOD. At lower k values the power of the mock catalogues decreases, as expected for any ΛCDM cosmology with typical values from *Wilkinson Microwave Anisotropy Probe* (WMAP) or *Planck* measurements. The power of the DR10 galaxy sample for the NGC decreases as well, but the SGC increases having extra power compared to the NGC. Tojeiro et al. (2014) have looked at the differences between NGC and SGC data in terms of systematics and found that none of the systematic contributions analysed in the CMASS sample has a significant impact in the LOWZ data. Tojeiro et al. (2014) found that the differences between the two Galactic caps are reduced in DR11 and are compatible with one another, given the expected variance computed from the mocks.

In the right-hand panel of Fig. 6 we show the two-point correlation function of the DR10 LOWZ galaxy sample both for the NGC (blue solid circles) and SGC (green solid). The DR11 values are set as open circles. We have used the Landy & Szalay (1993) esti-

imator, including FKP weights as it reduces the variance also in the correlation function. The error bars are the sample errors computed from the mock catalogues and the values of the mean of the mocks are shown as solid lines. The excess power of the SGC at low k translates into a higher values of the correlation function at a wide range of scales.

We present the values of the DR10 LOWZ power spectrum and correlation function, and their covariance matrices in the appendix of the paper. The mocks for LOWZ DR10 will be made publicly available online.⁶ These mocks have been used by the BOSS collaboration in analysis of the large scale of the LOWZ sample and the BAO peak position (Anderson et al. 2014; Sánchez et al. 2014; Tojeiro et al. 2014). The elements of covariance matrices estimated from a finite set of mocks have uncertainties that depend on the number of mocks. These uncertainties translate into errors in the inverse covariance matrices and likelihood estimators. Since our suite consists of 1000 mocks these errors are expected to be small in most cases, and are of order few per cent for 1000 mocks using 30 bins. For a detailed accounting for this errors see Percival et al. (2013).

6 CONCLUSION

We have created 1000 mock galaxy catalogues for the BOSS LOWZ DR10 and DR11 galaxy sample. These mock catalogues have been produced following the PTHalos method developed in Manera et al. (2013), but with significant differences. We have created 500 particle dark matter fields using a 2LPT code and obtained haloes in those fields by FoF method with the appropriate linking length. The mass of the haloes has been ranked and masses reassigned to match the Tinker et al. (2008) mass function. These PTHalos have been populated with galaxies. For each matter field we can fit two full LOWZ footprints without overlap, resulting in a 1000 mocks for both the NGC and the SGC. Redshift-space distortions are included through peculiar velocities.

In contrast to previous mocks these have been created allowing for a variable HOD as a function of redshift, automatically matching the number density of galaxies. The mocks were created by fitting simultaneously the measured clustering and number density, with no need for applying a posterior subsampling of galaxies. We have implemented the DR10 and DR11 LOWZ masks to the mock

⁶ www.marcmanera.net/mocks/

catalogues, including small vetoed areas due to bright stars or other effects like bad photometry and target completeness. We have also included close pair corrections, and redshift failures. For the fitting procedure and HOD dependence on number density see Section 4.3. The 1000 LOWZ galaxy catalogues have been used in the analysis of the baryon acoustic peak position (Anderson et al. 2014) and shape of the correlation function (Sánchez et al. 2014). In the appendix we present the LOWZ DR10 correlation function covariance matrix.

Mock galaxy catalogues for the BOSS CMASS galaxy sample ($0.43 < z < 0.7$) have also been upgraded from DR9 (Manera et al. 2013) to DR10 and DR11, keeping the same HOD but repopulating the haloes and applying the DR10 and DR11 footprints, completeness masks, and $n(z)$ fit as in Section 3. These mocks have been used in studying the clustering of red and blue galaxies (Ross et al. 2014), the accuracy of fitting methods (Vargas-Magana et al. 2014), and the analysis of the large-scale clustering and its cosmological implications, including the BAO position, anisotropic clustering (Chuang et al. 2013; Anderson et al. 2014; Samushia et al. 2014; Sánchez et al. 2014).

The DR10 LOWZ and CMASS mocks will be publicly available online.⁵

ACKNOWLEDGEMENTS

MM and WJP acknowledge support from European Research Council, through grant ‘MDEPUGS’. MM is very thankful to Ramin A. Skibba and Bob Nichol for useful comments and suggestions. Funding for SDSS-III has been provided by the Alfred P. Sloan Foundation, the Participating Institutions, the National Science Foundation, and the US Department of Energy Office of Science. The SDSS-III web site is <http://www.sdss3.org/>.

SDSS-III is managed by the Astrophysical Research Consortium for the Participating Institutions of the SDSS-III Collaboration including the University of Arizona, the Brazilian Participation Group, Brookhaven National Laboratory, University of Cambridge, Carnegie Mellon University, University of Florida, the French Participation Group, the German Participation Group, Harvard University, the Instituto de Astrofísica de Canarias, the Michigan State/Notre Dame/JINA Participation Group, Johns Hopkins University, Lawrence Berkeley National Laboratory, Max Planck Institute for Astrophysics, Max Planck Institute for Extraterrestrial Physics, New Mexico State University, New York University, Ohio State University, Pennsylvania State University, University of Portsmouth, Princeton University, the Spanish Participation Group, University of Tokyo, University of Utah, Vanderbilt University, University of Virginia, University of Washington, and Yale University.

Part of the numerical computations and analyses of this paper made use of the Sciama High Performance Compute (HPC) cluster which is supported by the ICG, SEPNet, and the University of Portsmouth; and of the COSMOS/Universe supercomputer, a UK-CCC facility supported by HEFCE and STFC in cooperation with CGI/Intel.

REFERENCES

- Anderson L. et al., 2012, *MNRAS*, 427, 3435
 Anderson L. et al., 2014, *MNRAS*, 441, 24
 Angulo R. E., White S. D. M., Springel V., Henriques B., 2014, *MNRAS*, 442, 2131
 Angulo R. E., Baugh C. M., Frenk C. S., Lacey C. G., 2014, *MNRAS*, 442, 3256
 Berlind A. A., Weinberg D. H., 2002, *ApJ*, 575, 587
 Blake C., Collister A., Lahav O., 2008, *MNRAS*, 385, 1257
 Brown M. J. I. et al., 2008, *ApJ*, 682, 937
 Bryan G. L., Norman M. L., 1998, *ApJ*, 495, 80
 Chuang C.-H. et al., 2013, preprint ([arXiv:1312.4889](https://arxiv.org/abs/1312.4889))
 Coupon J. et al., 2012, *A&A*, 542, 5
 Davis M., Efstathiou G., Frenk C. S., White S. D. M., 1985, *ApJ*, 292, 371
 Dawson K. S. et al., 2013, *AJ*, 145, 10
 de la Torre S., Peacock J. A., 2013, *MNRAS*, 435, 743
 Eisenstein D. J. et al., 2001, *AJ*, 122, 2267
 Eisenstein D. J. et al., 2011, *AJ*, 142, 72
 Feldman H. A., Kaiser N., Peacock J. A., 1994, *ApJ*, 426, 23 (FKP)
 Fukugita M. et al., 1996, *AJ*, 111, 1748
 Gunn J. E. et al., 1998, *AJ*, 116, 3040
 Gunn J. E. et al., 2006, *AJ*, 131, 2332
 Hill G. J., Gebhardt K., Komatsu E., MacQueen P. J., 2004, in Allen R. E., Nanopoulos D. V., Pope C. N., eds, *AIP Conf. Proc. Vol. 743, The New Cosmology: Conference on Strings and Cosmology; The Mitchell Symposium on Observational Cosmology*. Am. Inst. Phys., New York, p. 224
 Hong G. et al., 2014, *MNRAS*, 441, 2398
 Kitaura F.-S., Heß S., 2013, *MNRAS*, 435, L78
 Kulkarni G. V., Nichol R. C., Sheth R. K., Seo H., Eisenstein D. J., Gray A., 2007, *MNRAS*, 378, 1196
 Landy S. D., Szalay A. S., 1993, *ApJ*, 412, 64
 Laurejis R. et al., 2011, preprint ([arXiv:1110.3193](https://arxiv.org/abs/1110.3193))
 Levi M. et al., 2013, preprint ([arXiv:1308.0847](https://arxiv.org/abs/1308.0847))
 LSST Science Collaboration 2009, preprint ([arXiv:0912.0201](https://arxiv.org/abs/0912.0201))
 Mandelbaum R., Seljak U., Kauffmann G., Hirata C. M., Brinkmann J., 2006, *MNRAS*, 368, 715
 Manera M. et al., 2013, *MNRAS*, 428, 1036
 Monaco P., Theuns T., Taffoni G., 2002, *MNRAS*, 331, 587
 Monaco P., Sefusatti E., Borgani S., Croce M., Fosalba P., Sheth R. K., Theuns T., 2013, *MNRAS*, 433, 2389
 Nelder J. A., Mead R., 1965, *Comp. J.*, 7, 308
 Padmanabhan N., White M., Norberg P., Porciani C., 2009, *MNRAS*, 397, 186
 Parejko J. K. et al., 2013, *MNRAS*, 429, 98
 Peacock J. A., Smith R. E., 2000, *MNRAS*, 318, 1144
 Percival W. J. et al., 2013, *MNRAS*, submitted
 Pheleps S., Peacock J. A., Meisenheimer K., Wolf C., 2006, *A&A*, 457, 145
 Reid B. et al., 2012, *MNRAS*, 426, 2179
 Ross A. J. et al., 2012, *MNRAS*, 424, 564
 Ross A. J. et al., 2014, *MNRAS*, 437, 1109
 Samushia L. et al., 2013, *MNRAS*, 429, 1514
 Samushia L. et al., 2014, *MNRAS*, 439, 3504
 Sánchez A. G. et al., 2014, *MNRAS*, 440, 2692
 Scoccimarro R., Sheth R. K., Hui L., Jain B., 2001, *ApJ*, 546, 20
 Scoccimarro R., Sheth R. K., 2002, *MNRAS*, 329, 629
 Tassev S., Zaldarriaga M., Eisenstein D. J., 2013, *J. Cosmol. Astropart. Phys.*, 06, 036
 Tinker J. L., Kravtsov A. V., Klypin A., Abazajian K., Warren M. S., Yepes G., Gottloeber S., Holz D. E., 2008, *ApJ*, 688, 709
 Tinker J. L., Leauthaud A., Bundy K., George M. R., Behroozi P., Massey R., Rhodes J., Wechsler R. H., 2013, *ApJ*, 778, 93
 Tojeiro R. et al., 2012, *MNRAS*, 424, 2339
 Tojeiro R. et al., 2014, *MNRAS*, 440, 2222
 Van Daalen M. P., Schaye J., Booth C. M., Vecchia C. D., 2011, *MNRAS*, 415, 3649
 Vargas-Magana M. et al., 2014, *MNRAS*, 445, 2
 Wake D. et al., 2008, *MNRAS*, 387, 1045
 White M. et al., 2011, *ApJ*, 728, 126
 White M., Tinker J. L., McBride C. K., 2014, *MNRAS*, 437, 2594
 Xu X., Cuesta A. J., Padmanabhan N., Eisenstein D. J., McBride C. K., 2013, *MNRAS*, 431, 2834
 Zheng Z., Coil A. L., Zehavi I., 2007, *ApJ*, 667, 760
 Zheng Z., Zehavi I., Eisenstein D. J., Weinberg D. H., Jing Y. P., 2009, *ApJ*, 707, 554

APPENDIX A

Table A1. Covariance matrices of the spherically averaged correlation function $\xi(s)$ for the LOWZ DR10 NGC (top) and SGC (bottom), derived from 1000 mock galaxy catalogues. The first column and the first row of each subparts indicate with integers the centre of the bins in h^{-1} Mpc. Since the covariance matrix is symmetric only the lower half is displayed, and its values, for clarity, multiplied by 10^6 .

C(r1,r2)	30	38	46	54	62	70	78	86
30	32.15							
38	23.15	21.58						
46	15.69	15.86	15.52					
54	11.29	11.69	12.27	12.37				
62	8.384	8.821	9.545	10.12	10.42			
70	6.186	6.786	7.479	8.015	8.698	8.879		
78	5.013	5.452	6.112	6.504	7.085	7.511	7.74	
86	4.142	4.437	4.936	5.268	5.718	6.068	6.576	6.736
94	3.112	3.244	3.691	3.97	4.303	4.587	5.091	5.475
102	2.479	2.526	2.88	2.978	3.251	3.542	3.976	4.306
110	2.118	2.019	2.175	2.223	2.419	2.674	2.967	3.209
118	1.544	1.516	1.66	1.694	1.808	1.962	2.158	2.352
126	1.068	1.204	1.341	1.376	1.406	1.572	1.737	1.878
134	0.7244	0.8605	1.002	1.04	1.028	1.205	1.367	1.451
142	0.445	0.6053	0.7028	0.755	0.7507	0.8816	1.004	1.054
150	0.2411	0.387	0.4769	0.539	0.5401	0.6727	0.788	0.8107
C(r1,r2)	94	102	110	118	126	134	142	150
94	5.405							
102	4.453	4.527						
110	3.355	3.634	3.697					
118	2.456	2.735	2.996	3.145				
126	1.933	2.151	2.464	2.743	3.013			
134	1.505	1.675	1.965	2.257	2.625	2.874		
142	1.142	1.267	1.511	1.745	2.081	2.435	2.595	
150	0.9066	0.9725	1.175	1.364	1.655	1.987	2.224	2.351
C(r1,r2)	30	38	46	54	62	70	78	86
30	88.16							
38	64.43	60.73						
46	46.3	47.45	48.32					
54	31.59	34.57	37.63	37.47				
62	22.36	24.87	27.6	28.97	27.87			
70	16.61	18.52	20.92	22.38	22.84	23.49		
78	12.62	14.	15.86	17.49	18.24	19.44	19.94	
86	10.01	11.11	12.17	13.61	14.06	15.13	16.58	17.06
94	7.674	8.367	8.902	10.17	10.58	11.59	12.97	14.26
102	5.459	5.619	5.887	7.01	7.602	8.493	9.906	11.18
110	4.166	3.76	3.783	4.482	5.065	5.691	6.794	7.997
118	3.224	3.056	3.02	3.224	3.587	3.975	4.75	5.717
126	2.576	2.477	2.275	2.214	2.578	2.94	3.514	4.247
134	1.27	1.109	1.153	1.215	1.705	2.064	2.476	3.051
142	0.004535	0.03784	0.3373	0.5719	1.084	1.364	1.764	2.213
150	-0.9506	-0.5445	-0.04525	0.1988	0.6778	1.04	1.389	1.789
C(r1,r2)	94	102	110	118	126	134	142	150
94	14.88							
102	12.37	12.9						
110	9.248	10.35	10.57					
118	6.905	8.08	8.722	9.293				
126	5.098	6.116	6.719	7.655	8.256			
134	3.662	4.599	5.144	6.05	6.983	7.645		
142	2.589	3.244	3.643	4.449	5.385	6.302	6.868	
150	2.005	2.394	2.605	3.227	4.12	4.917	5.789	6.43